SUPPORTING INFORMATION

Origin of Broad Emission Induced by Rigid Aromatic Ditopic Cations in Low-Dimensional Metal Halide Perovskites

Marta Morana,[a] Waldemar Kaiser,[b,] Rossella Chiara,[a] Benedetta Albini,[c] Daniele Meggiolaro,[b] Edoardo Mosconi,[b] Pietro Galinetto,[c] Filippo De Angelis,[b,d,e] Lorenzo Malavasi[a,]**

[a]Department of Chemistry and INSTM, University of Pavia, Via Taramelli 16, Pavia, 27100, Italy
[b]Computational Laboratory for Hybrid/Organic Photovoltaics (CLHYO), Istituto CNR di Scienze e Tecnologie Chimiche "Giulio Natta" (CNR-SCITEC), 06123 Perugia, Italy
[c]Department of Physics, University of Pavia, Via Bassi 6, Pavia, 27100, Italy
[d]Department of Chemistry, Biology and Biotechnology, University of Perugia and UdR INSTM, 06123 Perugia, Italy
[e]SKKU Institute of Energy Science and Technology (SIEST) Sungkyunkwan University, Suwon, Korea 440-746.

Corresponding Authors

Waldemar Kaiser, email: waldemar.kaiser@scitec.cnr.it;
Lorenzo Malavasi, email: lorenzo.malavasi@unipv.it; tel. +39 382 987921

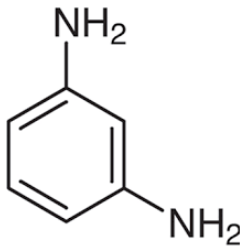

1,3-phenylenediammonium (1,3-PDA)

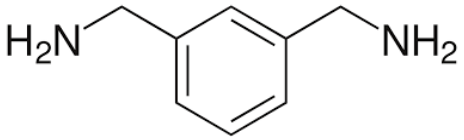

1,3-xylylenediamimonium (1,3-XDA)

1,4-phenylenediammonium (1,4-PDA)

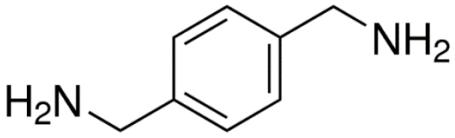

1,4-xylylenediamimonium (1,4-XDA)

Figure S1. Chemical structure of the diamines used in for the synthesis of Pb-Cl perovskites.

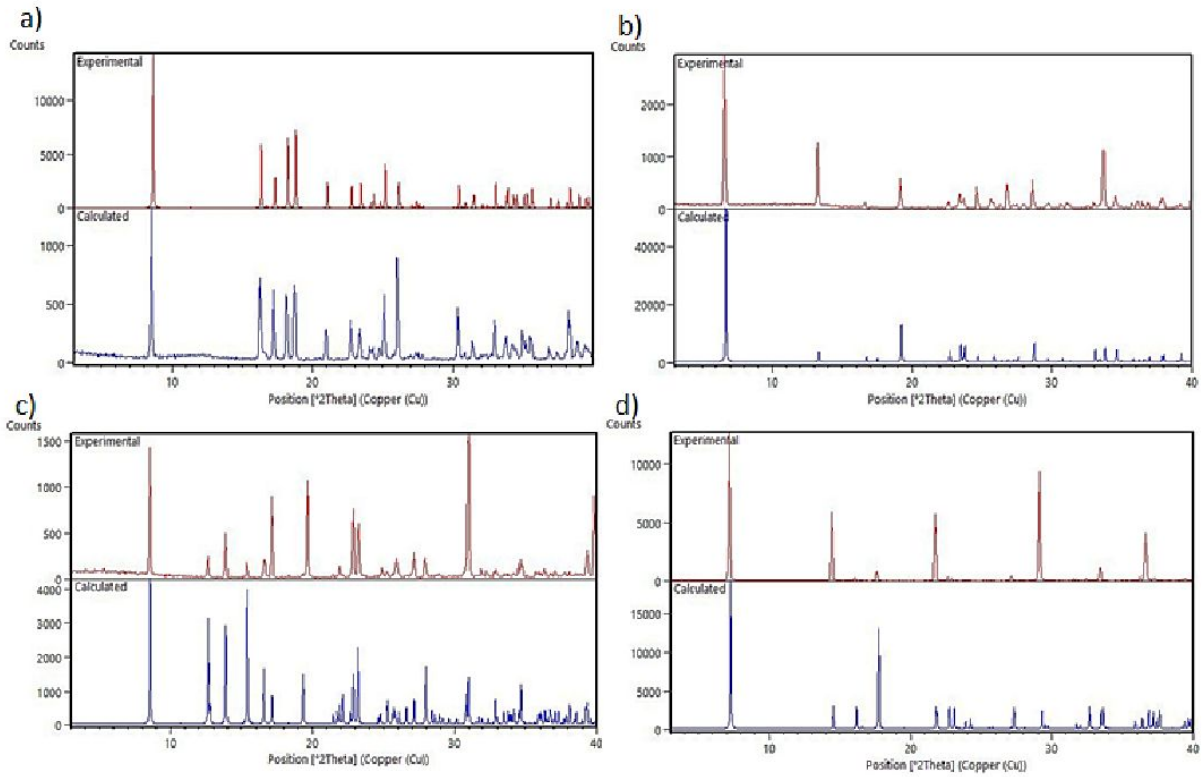

Figure S2. XRD powder patterns (red) of a) (1,3-PDA)$PbCl_4$, b) $(1,3\text{-XDA})_2PbCl_6$, c) (1,4-PDA)Pb_2Cl_6, d) (1,4-XDA)$PbCl_4$ superimposed to the calculated patterns from SC-XRD (blue) after exposing the samples to laboratory air for one week.

Materials and methods

Synthesis

Single crystals of (1,3-PDA)$PbBr_4$, (1,4-PDA)$PbBr_4$, (1,3-XDA)$PbBr_4$ and (1,4-XDA)$PbBr_4$ were grown by dissolving a proper amount of lead(II) acetate powder in a large excess of 48% w/w aqueous HBr and 50% w/w aqueous H_3PO_2, heating the mixture to boiling point. After the solid dissolution, the stoichiometric amount of the solid diamine (liquid for the 1,3-XDA) was added. The crystals formation was obtained by a slow cooling down to room temperature at 2°C h^{-1}.

Single crystal and powder X-ray diffraction

Single crystal data collections (λ = 0.71073 Å) were performed using a Bruker D8 Venture with Cu and Mo microfocus X-ray sources and PHOTON II detector with Bruker APEX3 program. The Bruker SAINT software[1] was used for integration and data reduction, while absorption correction was performed using SADABS-2016/2[2]. Crystal structures (CCDC) were solved and refined using SHELXT 2014/5 and SHELXL 2018/3[3,4].

Photoluminescence and Absorption measurements

Photoluminescence: PL measurements were performed by means of a NANOLOG FL3-2iHR spectrofluorometer, Horiba Scientific, equipped with a 450W Xenon lamp as excitation source and an iHR320 triple-grating turret spectrometer as excitation monochromator. A single channel photomultiplier tube was used as detector.

Absorption: RS spectra were acquired in the wavelength range 300-800 nm directly on the powders by using a Jasco V-750 spectrophotometer, equipped with an integrating sphere (Jasco ISV-922).

Computational Details

Geometry optimization of all structures, both in the ground state and in triplet state, have been performed using the freely available CP2K software package, using the hybrid exchange-correlation functional PBE0 with α=0.25, including van der Waals interactions with the DFT-D3 scheme with Becke-Johnson damping.[5–8] Kohn-Sham orbitals are expanded in a double-zeta basis set (DZVP-MOLOPT) in combination with the norm-conserving Goedecker-Teter-Hutter (GTH) pseudopotentials, and a cutoff of 300 Ry for expansion of the electron density in plane waves.[9,10] The auxiliary density matrix method with the cFIT auxiliary basis set was applied to accelerate the optimization of ionic positions within hybrid functional calculations.[11]

Emission energies of the optimized geometries were refined using the PBE0 functional with α = 0.25, including spin-orbit coupling (SOC), and DFT-D3 dispersion corrections within the Quantum Espresso package to correct for spin-orbit coupling effects due to the heavy Pb ions.[5,12] We used full relativistic norm-conserving pseudopotentials (Pb, 22 electrons, $5s^2$, $5p^6$, $5d^{10}$, $6s^2$, $6p^2$; Cl, 7 electrons, $3s^2$, $3p^5$; Br, 7 electrons, $4s^2$, $4p^5$; N, 5 electrons, $2s^2$, $2p^3$; C, 4 electrons, $2s^2$, $2p^2$; H, 1 electron, $1s^1$) with a cutoff on the wave functions of 40 Ry and 80 Ry on the Fock grid.

Defect formation energies (DFE) and thermodynamic ionization levels (TIL) were calculated as follows:

$$\mathrm{DFE}[\mathrm{X^q}] = \mathrm{E}[\mathrm{X^q}] - \mathrm{E}[\mathrm{prist}] - \sum_{\mathrm{i}} \mathrm{n_i}\mu_{\mathrm{i}} + \mathrm{q}(\mathrm{E_{VBM}} + \mathrm{E_F}) + \mathrm{E^q_{corr}} \quad (1)$$

$$\mathrm{TIL}[\mathrm{q/q'}] = \frac{\mathrm{DFE}[\mathrm{X^q}] - \mathrm{DFE}[\mathrm{X^{q'}}]}{q' - q} \quad (2)$$

where $E[X^q]$ is the energy of the defective supercell with defect X in charge state q, $E[prist]$ is the energy of the pristine supercell, n_i and μ_i are the number and chemical potential of the added and subtracted species, respectively, E_{VBM} and E_F are the valence band energy and the Fermi energy, respectively, and E^q_{corr} are electrostatic potential corrections due to the finite size of the supercell.[13,14] Electrostatic finite-size effects have been accounted for using the Freysoldt-Neugebauer-Van de Walle approach as implemented in the sxdefectalign code.[15]

Static dielectric constants were obtained using the density functional perturbation theory (DFPT) in the Vienna ab initio simulation package (VASP), with PBE exchange-correlation functional and the projector-augmented wave (PAW) method using a 300 eV plane-wave cutoff and converged k-space sampling for each compound based upon a tightly converged electronic wavefunction (within 10^{-8} eV).[16–19]

Table S1. Static dielectric constants for the bromide and chloride perovskite compounds from DFPT based on the PBE level of theory.

Compound	**Static Dielectric Constant**
(1,3-PDA)$PbBr_4$	14.0
(1,4-PDA)$PbBr_4$	10.9
(1,4-XDA)$PbBr_4$	8.1
(1,3-PDA)$PbCl_4$	12.7

(1,3-PDA)Pb_2Cl_6	12.6
$(1,3\text{-XDA})_2PbCl_6$	6.2
(1,4-XDA)$PbCl_4$	6.0

Additional Plots

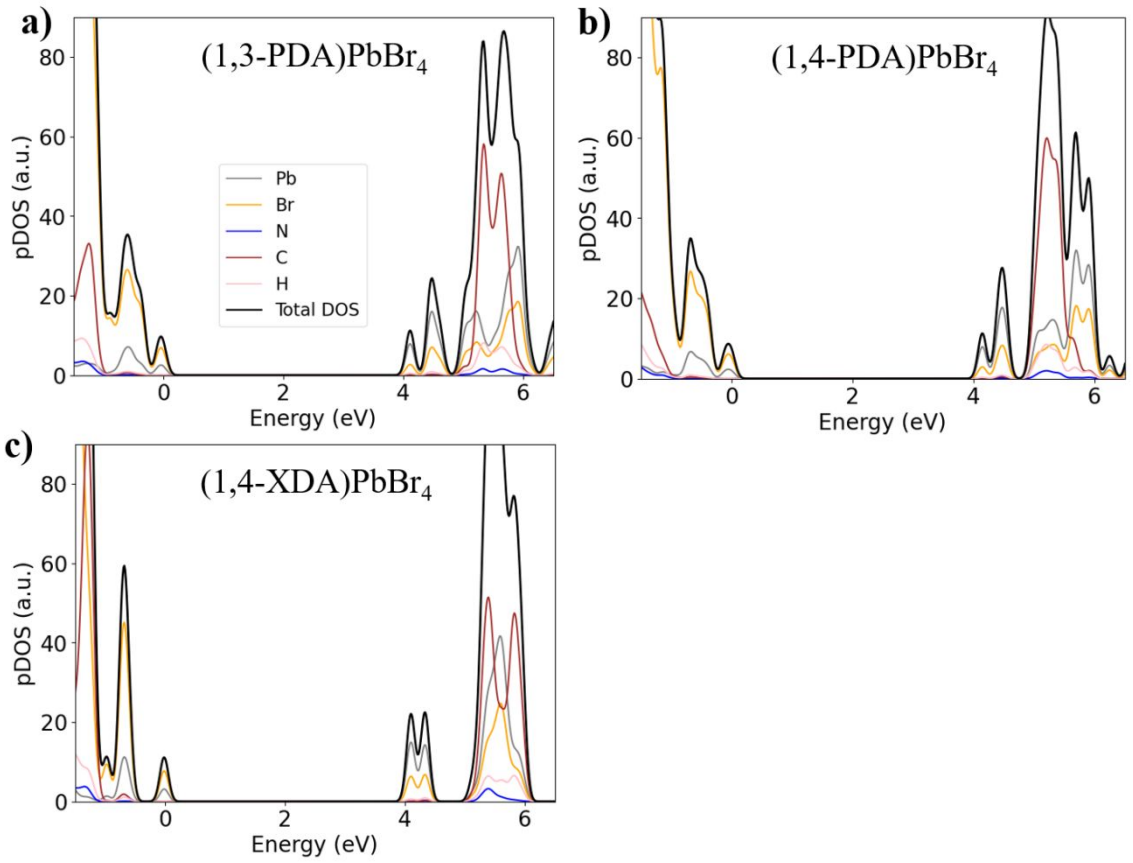

Figure S3. Projected density of states (pDOS) for investigate bromine-based 2D perovskites in the electronic ground state at PBE0 level of theory with α=0.25. The color code for all curves is given in the legend of panel a.

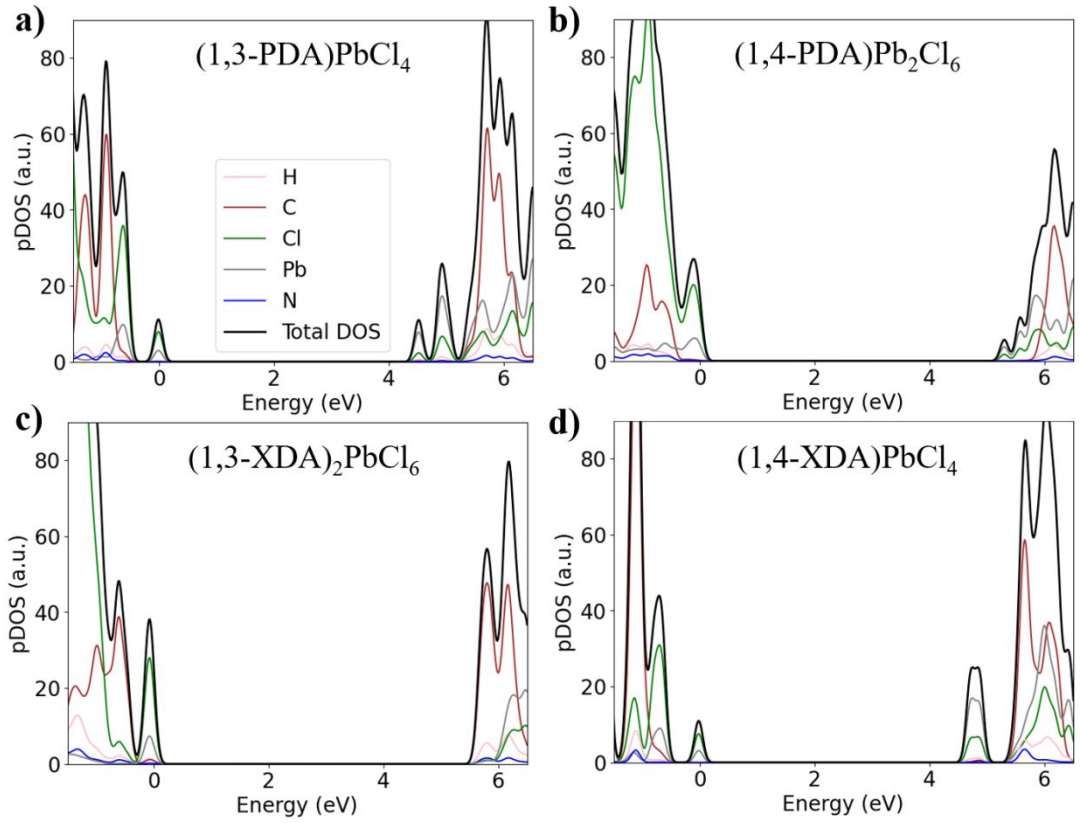

Figure S4. Projected density of states (pDOS) for investigate chlorine-based perovskites in the electronic ground state at PBE0 level of theory with α=0.25. The color code for all curves is given in the legend of panel a.

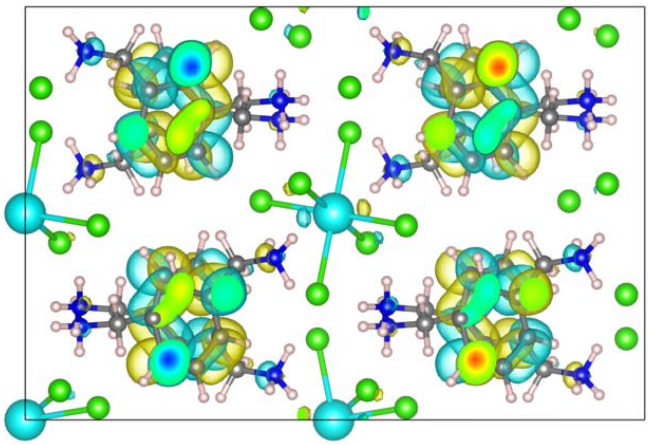

Figure S5. Visualization of lowest unoccupied molecular orbital (LUMO) for the 0D-perovskitoid (1,3-XDA)$_2$PbCl$_6$. The LUMO is delocalized along the 1,3-XDA cations, as expected from the pDOS, Figure S1c.

Table S2. Experimental band gap and theoretical band gap energies calculated on the PBE0 level of theory in units of eV.

Perovskite	**Exp. gap**	**Theor. gap**
(1,3-PDA)$PbBr_4$	~3	4.11
(1,4-PDA)$PbBr_4$	~3	4.14
(1,4-XDA)$PbBr_4$	~3	4.09
(1,3-PDA)$PbCl_4$	3.53	4.53
(1,4-PDA)Pb_2Cl_6	3.92	5.30
$(1,3\text{-XDA})_2PbCl_6$	3.87	5.66
(1,4-XDA)$PbCl_4$	3.51	4.69

References

(1) *Bruker. SAINT*; Bruker AXS Inc., 2015.
(2) *Bruker. SADABS*; Bruker AXS Inc.: Madison, WI, USA, 2016.
(3) Sheldrick, G. M. SHELXT – Integrated Space-Group and Crystal-Structure Determination. *Acta Cryst A* **2015**, *71* (1), 3–8. https://doi.org/10.1107/S2053273314026370.
(4) Sheldrick, G. M. Crystal Structure Refinement with SHELXL. *Acta Cryst C* **2015**, *71* (1), 3–8. https://doi.org/10.1107/S2053229614024218.
(5) Grimme, S.; Antony, J.; Ehrlich, S.; Krieg, H. A Consistent and Accurate *Ab Initio* Parametrization of Density Functional Dispersion Correction (DFT-D) for the 94 Elements H-Pu. *The Journal of Chemical Physics* **2010**, *132* (15), 154104. https://doi.org/10.1063/1.3382344.
(6) Kühne, T. D.; Iannuzzi, M.; Del Ben, M.; Rybkin, V. V.; Seewald, P.; Stein, F.; Laino, T.; Khaliullin, R. Z.; Schütt, O.; Schiffmann, F.; Golze, D.; Wilhelm, J.; Chulkov, S.; Bani-Hashemian, M. H.; Weber, V.; Borštnik, U.; Taillefumier, M.; Jakobovits, A. S.; Lazzaro, A.; Pabst, H.; Müller, T.; Schade, R.; Guidon, M.; Andermatt, S.; Holmberg, N.; Schenter, G. K.; Hehn, A.; Bussy, A.; Belleflamme, F.; Tabacchi, G.; Glöß, A.; Lass, M.; Bethune, I.; Mundy, C. J.; Plessl, C.; Watkins, M.; VandeVondele, J.; Krack, M.; Hutter, J. CP2K: An Electronic Structure and Molecular Dynamics Software Package - Quickstep: Efficient and Accurate Electronic Structure Calculations. *J. Chem. Phys.* **2020**, *152* (19), 194103. https://doi.org/10.1063/5.0007045.
(7) Adamo, C.; Barone, V. Toward Reliable Density Functional Methods without Adjustable Parameters: The PBE0 Model. *The Journal of Chemical Physics* **1999**, *110* (13), 6158–6170. https://doi.org/10.1063/1.478522.
(8) Grimme, S.; Ehrlich, S.; Goerigk, L. Effect of the Damping Function in Dispersion Corrected Density Functional Theory. *J. Comput. Chem.* **2011**, *32* (7), 1456–1465. https://doi.org/10.1002/jcc.21759.
(9) VandeVondele, J.; Hutter, J. Gaussian Basis Sets for Accurate Calculations on Molecular Systems in Gas and Condensed Phases. *The Journal of Chemical Physics* **2007**, *127* (11), 114105. https://doi.org/10.1063/1.2770708.
(10) Goedecker, S.; Teter, M.; Hutter, J. Separable Dual-Space Gaussian Pseudopotentials. *Phys. Rev. B* **1996**, *54* (3), 1703–1710. https://doi.org/10.1103/PhysRevB.54.1703.
(11) Guidon, M.; Hutter, J.; VandeVondele, J. Auxiliary Density Matrix Methods for Hartree−Fock Exchange Calculations. *J. Chem. Theory Comput.* **2010**, *6* (8), 2348–2364. https://doi.org/10.1021/ct1002225.
(12) Giannozzi, P.; Baroni, S.; Bonini, N.; Calandra, M.; Car, R.; Cavazzoni, C.; Ceresoli, D.; Chiarotti, G. L.; Cococcioni, M.; Dabo, I.; Corso, A. D.; Gironcoli, S. de; Fabris, S.; Fratesi, G.; Gebauer, R.; Gerstmann, U.; Gougoussis, C.; Kokalj, A.; Lazzeri, M.; Martin-Samos, L.; Marzari, N.; Mauri, F.; Mazzarello, R.; Paolini, S.; Pasquarello, A.; Paulatto, L.; Sbraccia, C.; Scandolo, S.; Sclauzero, G.; Seitsonen, A. P.; Smogunov, A.; Umari, P.; Wentzcovitch, R. M. QUANTUM ESPRESSO: A Modular and Open-Source Software Project for Quantum Simulations of Materials. *Journal of Physics: Condensed Matter* **2009**, *21* (39), 395502. https://doi.org/10.1088/0953-8984/21/39/395502.
(13) Freysoldt, C.; Grabowski, B.; Hickel, T.; Neugebauer, J.; Kresse, G.; Janotti, A.; Van De Walle, C. G. First-Principles Calculations for Point Defects in Solids. *Rev. Mod. Phys.* **2014**, *86* (1), 253–305. https://doi.org/10.1103/RevModPhys.86.253.
(14) Meggiolaro, D.; De Angelis, F. First-Principles Modeling of Defects in Lead Halide Perovskites: Best Practices and Open Issues. *ACS Energy Lett.* **2018**, *3* (9), 2206–2222. https://doi.org/10.1021/acsenergylett.8b01212.

(15) Freysoldt, C.; Neugebauer, J.; Van De Walle, C. G. Fully *Ab Initio* Finite-Size Corrections for Charged-Defect Supercell Calculations. *Phys. Rev. Lett.* **2009**, *102* (1), 016402. https://doi.org/10.1103/PhysRevLett.102.016402.
(16) Baroni, S.; De Gironcoli, S.; Dal Corso, A.; Giannozzi, P. Phonons and Related Crystal Properties from Density-Functional Perturbation Theory. *Rev. Mod. Phys.* **2001**, *73* (2), 515–562. https://doi.org/10.1103/RevModPhys.73.515.
(17) Kresse, G.; Furthmüller, J. Efficient Iterative Schemes for *Ab Initio* Total-Energy Calculations Using a Plane-Wave Basis Set. *Phys. Rev. B* **1996**, *54* (16), 11169–11186. https://doi.org/10.1103/PhysRevB.54.11169.
(18) Perdew, J. P.; Burke, K.; Ernzerhof, M. Generalized Gradient Approximation Made Simple. *Phys. Rev. Lett.* **1996**, *77* (18), 3865–3868. https://doi.org/10.1103/PhysRevLett.77.3865.
(19) Blöchl, P. E. Projector Augmented-Wave Method. *Phys. Rev. B* **1994**, *50* (24), 17953–17979. https://doi.org/10.1103/PhysRevB.50.17953.